20

Underwater hyperspectral imagery to create biogeochemical maps of seafloor properties

G. JOHNSEN, NTNU and UNIS, Norway, Z. VOLENT, SINTEF Fisheries and Aquaculture, Norway, H. DIERSSEN, NTNU, Norway, and University of Connecticut, USA, R. PETTERSEN, M. VAN ARDELAN and F. SØREIDE, NTNU, Norway, P. FEARNS, Curtin University, Australia, M. LUDVIGSEN, NTNU, Norway and M. MOLINE, University of Delaware, USA

Abstract: This chapter presents aspects of underwater hyperspectral imaging (UHI) techniques aimed at mapping biogeochemical objects of interest (OOI) on the seafloor. Case examples of instrument-carrying platforms and biogeochemical applications are given. We discuss how to create high resolution, georeferenced, optically corrected digital underwater maps of different habitats, minerals, substrates, and organisms. Corrections for platform speed and direction, inherent optical properties (IOP), optical path length, dynamic positioning, and pitch/roll/yaw are discussed in the context of using UHI-based optical fingerprints (i.e. spectral reflectance in visible wavelengths) of different targets to create maps that can help discriminate, identify, and quantify OOI, and provide statistical information on relevant seafloor features.

Key words: underwater hyperspectral imagery (UHI), underwater robotics, identifying biogeochemical OOI, digital maps of OOI, optical fingerprints.

20.1 Introduction

The seafloor is complex and dynamic, exhibiting large variability in biogeo-chemical composition over space and time.[1] Obtaining high quality maps of features on the seafloor is limited by traditional methods such as *in situ* diver surveys, ship-based acoustics (echosounders), benthic box core or 'grab' samples, epibenthic sledge and beam trawl samples, underwater pho-tography, and video towed from boat (drop camera, e.g. Boyd *et al.*, 2006;

---

[1] The techniques described in this chapter are currently patent pending.

508

Buhl-Mortensen *et al.*, 2010). These methods are often limited in spatial scale and are generally qualitative, requiring considerable human interpretation. New techniques have been developed that rely on the spectral signature of various features of the benthos. Different OOIs, from minerals to seagrass, absorb and reflect different portions of the visible spectrum giving them unique 'optical fingerprints'. By measuring the color reflecting off the seafloor using hyperspectral imaging, these optical fingerprints can be used to develop qualitative and quantitative maps of benthic habitats, substrates, minerals, and organisms.

Hyperspectral imagers can be deployed on satellites, suborbital aircraft, boats or on underwater platforms.[2] Remote sensing from satellites and airplanes has over the last decade provided a significant development in mapping different habitats on land and in the coastal ocean, such as desert/grassland ecotones and harmful algal blooms at the water surface (see Chapter 9, Ryan *et al.,* 2005; IOCCG, 2008; Johnsen *et al.*, 2009). There is a current need for similar detailed mapping and monitoring of biogeochemical OOI underneath the sea surface. Passive airborne remote sensing is possible in areas termed 'optically shallow,' where the spectral reflectance off the seafloor contributes to radiance measured above the sea surface and is defined by the water clarity, bottom depth, and bottom composition (Dierssen, 2011). Such techniques have been used to map corals, seagrass, kelp (Dierssen *et al.*, 2003; Phinn *et al.*, 2005; Volent *et al.*, 2007; Johnsen *et al.*, 2011), and a variety of sediments and other near-shore habitats (Mobley *et al.*, 2005; Klonowski *et al.*, 2007).

Most of the seafloor is optically deep and cannot be imaged with passive techniques that rely on sunlight. For such situations, UHI can be deployed on underwater vehicles, such as remotely operated vehicles (ROV) or autonomous underwater vehicles (AUV), and deployed in close proximity to the seafloor in order to systematically map the benthos over large areas. In contrast to passive remote sensors, underwater remote sensing requires active sensors using spectrally defined artificial light sources positioned close to the substrate for the benthic reflectance to be measured at high spatial and spectral resolution (Hochberg and Atkinson, 2003; Grahn and Geladi, 2007).

By using UHI instead of the 3-color RGB-based pictures and video, we can move toward automated identification of OOI. To do so, the reflectance spectrum $R(\lambda)$ of an OOI is used to classify the habitat. If the UHI is deployed at ocean depths devoid of sunlight, the OOI must be illuminated by an artificial light source. The light from the source is directed along a narrow beam toward the OOI. Light reflected from the OOI is altered

---

[2]   Johnsen, G, Inventor; Underwater Hyperspectral Imager (WO2009141622). http://www.wipo.int/pctdb/en/wo.jsp?WO=2009141622

spectrally and detected by the UHI. However, the water and its optical constituents also affect the spectrum of the detected light. Light is absorbed and scattered along the direct and reflected beams in relationship to the optical properties of the water column. The reflectance spectrum from the OOI will be modified by particles and other substances in the water column and should be considered when spectrally classifying the OOI.

In this chapter we will focus on the use of UHI to map and monitor the seafloor for biogeochemical OOI. We start (Section 20.1) with a brief examination of hyperspectral imagery at various spatial, spectral, radiometric, and temporal resolutions and further elucidate optical fingerprints in Sections 20.2 and 20.3 outlining the different underwater platforms for UHI technique. We describe the needs for controlled georeferencing, positioning, and the UHI sensor requirements in Sections 20.4 and 20.5 and present how we can optically process the imagery to classify OOI. Lastly, we present in Section 20.6 some examples of UHI-based biogeochemical mapping of seafloor, with potential applications for environmental agencies, oil, gas, and mining industries.

20.2   Underwater hyperspectral imaging (UHI) techniques

Here we go through the basic information regarding use of hyper spectral imagery underwater to obtain specific optical fingerprints of OOI.

20.2.1   Benefits and resolutions of UHI

The benefit of placing hyperspectral imaging sensors on underwater platforms, in close proximity to the OOI, can be evaluated by considering four categories of resolution, namely:

1. Spatial (image pixel size),
2. Spectral (human eye vs broadband vs hyperspectral sensors),
3. Radiometric (bits per pixel and dynamic range), and
4. Temporal (re-visit time).

Spatial resolution

The spatial resolution available from an imager is related to the distance from the target and the signal-to-noise ratio of the sensor. Polar-orbiting sensors, deployed on satellites, typically view the entire earth from an altitude of approximately 800 km with a ground resolution of hundreds to thousands of meters providing complete global coverage in 1–2 days. In contrast to these space-borne sensors, a similar technology may be employed to map smaller regions using sensors mounted on aircraft, boats, or underwater vehicles. Airborne remote sensing hyperspectral instruments are typically flown at

altitudes ranging from about 1.5 to 3 km when targeting coastal and shallow water regions, providing a spatial resolution in the range 1–4 m depending on the architecture of the HI, its settings/optics, altitude, and speed (Davis *et al.*, 2006; Klonowski *et al.*, 2007; Volent *et al.*, 2007). A UHI mounted on underwater vehicles scanning OOI at a distance of 2 m above the seafloor will typically obtain a spatial resolution of approximately 2 mm. Different scales of mapping can be used to address different scientific and environmental questions and also be simultaneous and complementary to one another. Satellite imagery obtained across the entire ocean surface is ideal for addressing questions related to climate and global biogeochemistry, as well as large-scale features of optically shallow water ecosystems (Bierwirth *et al.*, 1993; Dierssen *et al.*, 2010; Lee *et al.*, 2010). The fine-scale features observable with UHI are ideal for mapping underwater habitats that comprise diverse mixtures of OOI varying on sub-meter scales. The technique is also useful for edge-detection and delineating changing ecotone boundaries over time.

Spectral resolution

The human eye utilizes so-called red, green, and blue (RGB) photoreceptor cells (cones with peak absorbance at 420, 534, and 564 nm), which is the basis of the human trichromatic perception of colors (Plate XIX, upper image (see in the color plate section between pages 326 and 327)). Artificial sensing systems, as well as colored image display systems such as television, computers, digital camera/video systems, and image scanners, have thus typically been based on the RGB color model. These RGB images are called 'pseudo-true' color because they use bands that are centered in the blue (450 nm), green (550 nm), and red (650 nm) portions of the visible spectrum and not the true spectral response of the human eye. For example, the spectral peak in light reflected from dense algal blooms or 'red tides' is not in the red region of the visible spectrum but closer to yellow at 570–580 nm. As phytoplankton become concentrated, the color shift observed from green to red is not due to any special optical properties of the algae but results from an overlap in spectral response of the eye's red and green cones (Dierssen *et al.*, 2006). While useful for human vision, however, spectral classification of standard RGB underwater imagery is often insufficient for distinguishing diverse bottom types (Gleason *et al.*, 2007).

In contrast to the human eye and simple trichromatic imaging systems, a multispectral imager (Plate XIX, mid image) is sensitive to more than 3 wavebands (colors), and when designed for remote sensing of the environment typically uses 10–20 wavebands in the ultraviolet, visible, and near-infrared regions of the electromagnetic spectrum. The traditional ocean color satellites, for example, commonly have only 6–7 wavebands spanning the visible spectrum designed to overlap with absorption features of oceanic

water, but have large gaps in spectral coverage (Dierssen, 2010). The only known organism group with true multispectral vision is the marine mantis shrimp, with an astounding spectral sensitivity of about 13 wavebands spanning 300 to over 700 nm (note that there are species-specific variations, Marshall and Oberwinkler, 1999; Marshall *et al.*, 2007).

Hyperspectral imagers, also called imaging spectrometers, typically detect light at approximately 1–5 nm spectral spacing and provide hundreds of wavebands across the visible spectrum, instead of only three afforded by the human eye (Plate XIX, lower image). Each hyperspectral pixel thus contains information representing a continuous spectrum, even though the pictorial representation of the data is presented as a three band, RGB image. The great advantage for imaging and detection purposes is that each image pixel and its highly detailed spectrum has the potential to discriminate subtle differences in spectral features, thus providing a means of classifying different OOI. Current work on airborne hyperspectral reflectance of corals, algae, seagrass, and sediment indicates that a spectral resolution of <10 nm might improve classification accuracy of unknown targets significantly relative to the RGB bands available on commercial cameras (Mobley *et al.*, 2005; Klonowski *et al.*, 2007; Gintert *et al.*, 2009; Gleason *et al.*, 2010; Fearns *et al.*, 2011). Numerical/statistical analysis of the OOI spectra provides an increased understanding of the natural variability in spectral characteristics of an OOI, beyond that which the 'eye' can see, which in turn aids in developing techniques to classify OOI automatically.

Compared to the trichromatic imaging system of the human eye, an HI can detect high spectral resolution 'optical fingerprints' that may be considered unique to a given OOI. Here we use the distinct spectral characteristics of salami sausage as an example to illustrate hyperspectral imaging of a biochemical sample (Plate XX (see in the color plate section between pages 326 and 327)). The constituents of salami, ranging from meat to fat, can be discriminated spectrally and used to classify many fine-scale features within the sausage. An image of salami, for example, shows fat with enhanced reflectance across visible wavelengths (white), meat with a more red/brown hue peaking in the red portion of the spectrum (600–650 nm), and various mixtures of both fat and meat. Such biochemical imaging can provide statistical information that can be used to determine the quality of product (e.g., percent fat content) or potentially classify the origin of the meats used in the product.

When we consider the application of HI to classification of OOI in the marine environment, the spectral information detected by the sensor is similar to the above example. Each constituent on the seafloor absorbs light of certain wavelengths and reflects light at other wavelengths. The spectral signature reflecting from the seafloor can be measured at high spectral resolution to discriminate different types and mixtures of bottom features.

Differently from the salami example in air, however, the seafloor is imaged through a layer of water – a highly absorbing and scattering medium. Hence, the optical constituents of the water column must be considered in the analysis of the optical fingerprints measured with a UHI. The color or spectral reflectance will be altered by the absorption and scattering properties of water molecules, as well as particles and dissolved matter within the water column. In layman terms, the imager will produce a different measurement depending on the distance to the target and whether the material is submerged in liquid resembling spring water, milk (highly scattering) or coffee (highly absorbing). Such corrections are incorporated into the analysis of the data and are considered further in Section 20.3.

Radiometric resolution (bit per pixel)

The bit per pixel (= bit depth) denotes the number of digital levels determining the radiometric precision of the measurement (giving the dynamic range). The UHI exemplified in this chapter has a rate of 8 bits per pixel giving 2^8 or 256 intensities at a given wavelength. Higher bit rates (e.g. 12–14-bit) are also possible for off-the-shelf imagers and other hyperspectral sensors (Lucke *et al.*, 2011). A major advantage of higher bit rates is the ability to sample a greater range of intensity. More bits provide a given image with better exposure control and color intensity dynamics. A large dynamic range is especially important for marine targets, which include both bright and very dark targets (Mouroulis *et al.*, 2012). However, greater radiometric resolution results in larger data files, which can be difficult to process and manipulate with standard computer systems.

Temporal resolution

For most polar-orbiting ocean color satellites, the re-visit time or 'temporal' resolution is on the scale of days, depending on sensor and orbital specifications. However, the actual temporal resolution is dependent on other environmental factors, such as cloud and ice cover, and seasonal light availability, which can limit imagery to weekly or monthly averages. A UHI is not limited by orbital constraints, light, or cloud/ice cover, and can be deployed with a temporal frequency that is required for the question under investigation. The temporal resolution necessary for mineral mapping, for example, is far less than that required for algal distributions that can vary at daily to hourly time scales or even less (Sosik *et al.*, 2003; Volent *et al.*, 2011). Routine surveys may also be employed to look for changes to benthic features due to industrial activities, environmental mapping and monitoring, or natural processes of interest. For a UHI sensor implemented on a given underwater platform, it is crucial to have high accuracy geolocalization to be able to re-visit a given site or OOI. Because of this, an ROV or AUV needs to use

a dynamic position system to monitor and re-visit large areas and to give detailed time-series of habitat development (see Section 20.4.2).

20.2.2   Optical fingerprints

The spectral reflectance or 'optical fingerprint' of different OOI on the seafloor is independent of the illumination and the water column properties (Plate XXI (see in the color plate section between pages 326 and 327)). Mathematically, it is described as the ratio of upwelling irradiance coming off the substrate, $E_u(\lambda)$, normalized to the spectral downwelling irradiance incident upon the substrate, $E_d(\lambda)$. In other words, it is a percentage of how much light at each wavelength is reflected off the substrate or OOI. For wavelengths that are highly absorbed, such as blue and red wavelengths in plant matter, the reflected color is generally green. Measurements of benthic reflectance can be done in the lab from cores or diver-collected specimens, or with a diver-operated spectrometer or imager. Because of the way light refracts through an air–water interface, lab-based measurements approximate the spectral shape of reflectance, but the absolute spectral magnitude may vary somewhat from the reflectance of submerged specimens. Diver-operated spectrometers or imagers can be employed to measure the benthic reflectance from OOI directly in the field without specimen collection.

Spectral reflectances (not spectral images) of a variety of seafloor features have already been measured and detected across a wide array of substrates, and can be incorporated into a spectral library (Mobley *et al.*, 2005). The radiative transfer model, Hydro Light (Sequoia Scientific, WA, USA), for example, contains idealized spectra for a variety of sediment types, seagrass, and other constituents. The spectral reflectance for different sediments increases monotonically from blue to red wavelengths, with a dip at 665 nm due to chlorophylls (Chl *a, b* and *c*) within the sediment (Dierssen *et al.*, 2010). However, the mineral content of the sediment, and the amount of biofilm on the sediment surface, can change the spectral properties over both temporal and spatial scales (Buonassissi and Dierssen, 2010, see Section 20.6).

## 20.3   UHI on different underwater platforms

We here discuss the use of UHI on moving underwater platforms as instrument carriers to obtain detailed OOI maps of seafloor. By using mobile underwater robots, there is a potential to map areas from 1 m^{-2} to 1000 km^{-2}.

20.3.1   UHI on remotely operated vehicles (ROV)

An ROV is a remotely operated vehicle that is deployed and tethered from a ship during the entire deployment. The tether (umbilical) provides both

power and communication to the vehicle. An advantage of using an ROV as a UHI platform is the on-line control of the instrument and collection of the data stream (Fig. 20.1a and 20.1b). Any problems with the acquired data can be diagnosed rapidly, and controls can be sent to the platform to adjust the settings on the instrument package. Because power is provided through the tether, there are virtually no constraints regarding the power payload.
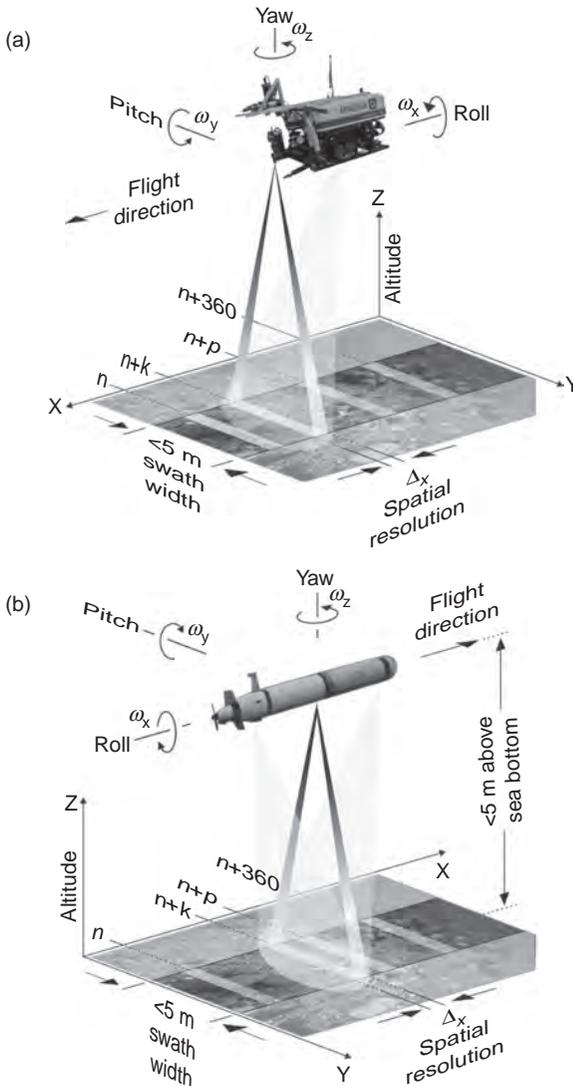
20.1 UHI deployed on (a) ROV (Sperre Subfighter 7500) or (b) on AUV (Hydroid Remus 600, Kongsberg Maritime) equipped with artificial light sources to illuminate OOI on seafloor.

This is particularly important when conducting active imaging that requires external light sources. Many different lamps with high power usage can be considered for deployment with the UHI mounted on an ROV. Moreover, ancillary sensors to measure water column optical properties, e.g. Wet Labs Ecopuck for Chl *a*, colored dissolved organic matter (CDOM) and total suspended matter (TSM) measurements of the water column and acoustic sensors to map bathymetry (multibeam echo sounder) or bottom substrate (side scan sonar) can also be readily implemented on the package (Moline *et al.*, 2005).

If a dynamic position (DP) system is provided on the ship (see Section 20.4.2), automation of DP control can be used to map the seafloor in predefined patterns, such as back and forth like a lawn mower, with high accuracy and precision. By using Ultra-short Baseline and Long Baseline navigation, the ROV platform can be driven with control over speed/direction, altitude, pitch, roll, and yaw and provide high quality images that can be merged into high resolution photomosaics of the entire sampling region (Singh *et al.*, 2004; Ludvigsen *et al.*, 2007). Hence, ROV-based UHI mapping can cover seafloor transects from 10 to 500 m of length, and high quality imagery can be produced.

A major disadvantage of using ROVs for deployment of the sensor is that the tether, which is generally 500–1000 m long, limits the aerial coverage. In addition, considerable time and cost are associated with deploying a fully operational vessel to tether the ROV during the entire deployment time. From an operational perspective, the ROV contains external thruster motors that can interfere with imaging potential. For example, if the UHI is close to a soft-bottom seafloor (e.g., loose, unconsolidated sediments), the thrusters may suspend sediments and reduce image quality. As DP systems improve with better control of the altitude, speed, and movement of the ROV (see Section 20.4.2), UHI quality will improve concurrently.

20.3.2   UHI on autonomous underwater vehicles (AUV)

An AUV is an autonomous underwater vehicle that can either be a glider or propeller-driven system. Autonomous gliders change buoyancy internally and profile the water column by converting a fraction of their vertical motion into horizontal velocity (Moline *et al.*, 2005). While useful for many oceanographic applications, gliders have very low power capacity and limited sustained sampling capabilities near the seafloor. As such, gliders are not ideal platforms for UHI and are not considered further here. Propeller-driven AUVs, in contrast, offer higher payloads than gliders and more systematic sampling capabilities that can be readily coupled with UHI. The AUV travels at speeds, typically between 1 and 5 knots, and samples over large distances without the constraints of a tether and ship-based crew.

Propeller-driven AUVs are found in different sizes and range classes. Small AUVs are typically 1.5–2 m in length, about 20 cm diameter and weighing 40–100 kg with a range of 100 km with diving limits to 100–500 m depth. The small AUV system is hand deployable by two people from a small boat, requiring a lower operating cost compared to an ROV (Moline *et al.*, 2005). Larger AUVs may be 3–5 m long, up to about 80 cm in diameter, weighing up to 900 kg, and can travel several hundred kilometers and to depths of 6000 m (e.g. REMUS 6000).With its high degree of speed/direction, altitude and pitch, roll, and yaw control, a large AUV may be the best platform for UHI mapping over large areas of seafloor. Predefined flight patterns (i.e. horizontally, zigzag or terrain-following at predefined altitudes) are possible to achieve with high precision, as well as the possibility of adaptive sampling (Blackwell *et al.*, 2007). Importantly, altitude control on AUVs makes mapping of the seafloor quite efficient.

Compared to towed cameras (Barker *et al.*, 1999), seafloor imaging from an AUV provides several improvements, such as:

(a) Targeting (precise positioning) of specific geolocalized OOI maps on the seafloor over larger areas 1–200 km range (Moline *et al*., 2005, 2007; Johnsen *et al.*, 2011, p. 541).
(b) Altitude and position control making it possible to map the seafloor at a close and constant distance at predefined speed (Moline *et al.*, 2007; Williams *et al.*, 2010).
(c) Ability to map very rough bottoms, vertical walls and complex structures.

The Seabed AUV is an example of a very stable optical imaging platform that has been used in a diverse range of oceanographic cruises, including coral reef characterization using photomosaic cameras and sonars (Singh *et al.*, 2004a, 2004b, Williams *et al.*, 2008). The commercial availability and versatility of AUVs make them a good platform for conducting routine UHI.

20.4   Sensor and navigational requirements

The following section outlines the hardware and software requirements for conducting high quality UHI on ROVs and AUVs.

20.4.1   UHI sensor requirements

The preferred sensor architecture for a hyperspectral imager (or imaging spectrometer) is the so-called 'push-broom' design, where the entire scan line is imaged synoptically by a line of sensors arranged perpendicularly

to the direction of imaging. The image of the spectrometer slit is projected on the ground and scanned forward with the motion of the sensor. The width of the scan in the cross-track direction is the cross-track field of view (CFOV). The slit image is dispersed by a spectrometer utilizing a two-dimensional detector array that records spectral information in the direction perpendicular to the slit.

Ocean targets provide critical challenges to spectrometer system design (Mourolis *et al.*, 2012):

1. There is a large dynamic range in reflectance measured by the sensor that can vary from 1% to 90% depending on the target of interest.
2. The fine spatial scale requires a high degree of spectrometer response uniformity.

An advantage to underwater imaging is that the desired signal is not overwhelmed by atmospheric scatter, and polarization sensitivity is not generally a problem.

The UHI sensor needs to be small (to fit into underwater robots) and have a pressure housing. A solid state UHI sensor is preferable, since no moving parts will minimize malfunction (cold and humid conditions may often be the situation in an underwater house) and reduce power demand to a minimum. Focusing capabilities on a UHI are challenging when considering an imager that changes distance from the OOI as it moves across the seafloor. The sensor can be deployed with a fixed predetermined focal plane and deployed at a fixed distance from the seabed. Dynamic focusing of the instrument is also a possibility, but difficult given the changing terrain and vehicle speeds.

The energy payload of an active UHI is largely driven by the high power demand of the underwater lamps compared to the UHI sensor itself. In the examples presented below, for example, two 35 W Halogen lamps use 6 Ah compared to the imager which uses only 0.17 Ah. Specifically designed light sources are needed to ensure that the OOI is well and evenly lit and receives all wavelengths needed for identification (see Section 20.6).

In addition, the ideal light source should be collimated and situated in such a manner as to avoid stray light scattering into the sensor. The UHI should ideally detect only those photons that have reflected off the target and have not been scattered into the detector from the water column alone.

20.4.2   Georeferencing and navigation

The push-broom technique used for the UHI relies on the navigational data to compile an image cube from each individual scan line. Data are also

georeferenced with absolute coordinates (Volent *et al.*, 2007).The accuracy of image georectification can be determined from comparisons to complementary data types collected on the platform, such as side scan sonar imagery or photomosaics (Ludvigsen *et al.*, 2007).The accuracy requirement for the resulting data determines the navigation equipment and survey procedures. Ideally, the position and orientation accuracy should match the UHI seabed resolution. The UHI sensor outlined in this chapter can provide millimeter seabed resolution. With the present state-of-the-art navigation equipment, such accuracy is not possible. It is, however, possible to get millimeter precision, whereby the relative position from one line to the next can be determined within millimeter resolution.

Georeferencing

The navigational data for the underwater vehicle on which the UHI is mounted are used for georeferencing the image cube. There are two main principles for underwater navigation: acoustic baseline positioning, and dead reckoning. The first is most common for ROVs, while the latter is more used for AUVs (Plate XXII (see in the color plate section between pages 326 and 327)).

Acoustic underwater navigation

Ultra-Short BaseLine (USBL) and Long BaseLine (LBL) are the dominant methods for ROV positioning. To achieve a global position using a USBL system a ship-mounted transceiver, a ship-mounted orientation sensor, and a GPS transponder mounted on the ROV are required, see Plate XXIIa. For LBL positioning, the system consists of an array of transponders placed on the seabed and a transceiver mounted on the ROV. With this system, the position can be obtained independently of the vessel sensors (Plate XXIIb). See Milne (1983) for additional explanations of the positioning principles.

Dead reckoning

Dead reckoning is a method for estimating the positioning where the initial position, heading, time, and velocity are used to calculate position. Mathematically, speed and acceleration are integrated over time to establish position estimates. Common sensors used for dead reckoning are gyro, Doppler Velocity Log (DVL), Inertial Measurement Unit (IMU), and Inertial Navigation System (INS).

Pitch roll yaw corrections

To correct the hyperspectral data for pitch, roll, and yaw for the UHI, we will start with the mathematical model for the system. In the equation below, ϕ

denotes roll, θ denote pitch and ψ denotes yaw angles of the UHI and the underwater robot (e.g. ROV or AUV).

$$
\begin{bmatrix} x \\ y \\ z \end{bmatrix}_{\text{absolute seabed data}} = \begin{bmatrix} x \\ y \\ z \end{bmatrix}_{\text{absolute instrument}_x} + R(\phi, \theta, \psi) \cdot \begin{bmatrix} x \\ y \\ z \end{bmatrix}_{\text{local}_x}
\qquad [20.1]
$$

The data from the UHI are collected in a local reference system, $[x\ y\ z]^{T}_{\text{local}}$. Using the absolute position of the instrument $[x\ y\ z]^{T}_{\text{absolute instrument}}$ and the rotation angles (ϕ, θ, ψ) of the instrument, the absolute coordinates of the seabed data points are determined. R denotes the rotation matrix. Using Euler notation the rotation matrix is:

$$
R(\phi, \theta, \psi) = \begin{bmatrix} \cos\psi - \cos\theta & -\sin\psi - \cos\phi + \cos\psi - \sin\theta - \sin\phi & \sin\psi - \sin\phi + \cos\psi - \cos\phi - \sin\theta \\ \sin\psi - \cos\theta & \cos\psi - \cos\phi + \sin\theta - \sin\theta - \sin\psi & -\cos\psi - \sin\phi + \sin\theta - \cos\phi \\ -\sin\theta & \cos\theta - \sin\phi & \cos\theta - \cos\phi \end{bmatrix}
$$

$$[20.2]$$

Dynamic positioning

The UHI typically has a rather narrow swath width (3–6 m), and many passes of the imager are required to build up a comprehensive map of the seafloor. For most applications, the platform is moved in a back and forth pattern similar to a lawn mower with lines that overlap in spatial domain. The amount of overlap between the lines is variable, but can be around 50% overlap for some applications. Precise maneuvering of the platform is required to produce low cross-track error, a stable heading, and consistent overlap between lines. For ROVs going at low velocities, this can be challenging and tedious for the ROV operator. An automatic maneuvering system, similar to autopilot or DP, increases the precision of maneuvering and hence the resulting data. AUVs have integrated controllers for vehicle heading, velocity, and cross-track error that allow for accurate survey lines.

20.5   Optical processing of hyperspectral imagery

Here we present information regarding the optical properties of the water column in relationship to UHI and processing of imagery.

20.5.1   Optical properties of the water column

The apparent optical properties (AOP) are dependent on both the medium and geometric structure of the light field (see Chapters 1 and 4).

The AOPs are measured with passive optical sensors, using the ambient light (sun) as light source. Two common AOPs for remote sensing purposes are the diffuse attenuation coefficient (K_d, m^{-1}) and ocean reflectance. While AOPs can be routinely measured (but hard to measure well), they are difficult to interpret quantitatively with respect to biogeochemical properties in the water column. In contrast, the IOPs depend only on the medium and its constituents, and are independent of the ambient light field. Since UHI imaging described here uses external light sources, it can be defined as an active optical technique. In contrast to passive AOP sensors, the active UHI can be used at night-time and at depth with no ambient light available (Johnsen *et al.*, 2011).

A UHI imager must be deployed at a distance from the substrate and cannot measure the true reflectance from the seafloor without the influence of the intervening water column. Hence, some knowledge of the optical properties of the water column must be incorporated into analysis of the imagery. The two IOPs commonly used for remote sensing and imaging include the absorption (*a*) and scattering (*b*) coefficients, which refer to the fraction of collimated light which is absorbed or scattered per unit distance within the medium (units 1/L or m^{-1}). Oceanic constituents that are primarily responsible for absorption of photons include water molecules, phytoplankton pigments, particulate detritus, and CDOM (Fig. 20.2). Pure water is increasingly effective at absorbing light at wavelengths greater than 550 nm and absorbs minimally in the blue and green portion of the visible spectrum. Conversely, CDOM absorbs maximally in the ultraviolet and blue portion of the spectrum, decreasing exponentially with wavelength at a rate that is related to the composition, or degradation state, of the material (see Chapter 5). Comprising primarily humic and fulvic acids released through the degradation of plant tissue, CDOM is most prevalent in coastal and estuarine waters with considerable riverine influence (Kirk, 1994; Blough and Del Vecchio, 2002). Non-living particulate material, called detritus or tripton, absorbs in a manner similar to CDOM and the two components are often modeled together with an exponential or hyperbolic model. Phytoplankton absorb light in a complex manner related to the composition and quantity of their photosynthetic pigments (Bricaud *et al.*, 2004; Johnsen *et al.*, 2011), but generally absorb strongly in the blue and red portions of the spectrum. Water molecules, salts, organic and inorganic particles, and bubbles provide strong contributions to light scattering in the ocean (Fig. 20.2).

Optical properties of the water column influence the radiance measured at the imager, and are important for quantitative analyses of the imagery. The greater distance the imager is from seafloor, the greater distortion the water column has on the measured radiance. At some threshold distance, the light coming off the seafloor can be attenuated below the sensor's detection limits, particularly at wavelengths highly absorbed by the water column (e.g. red).
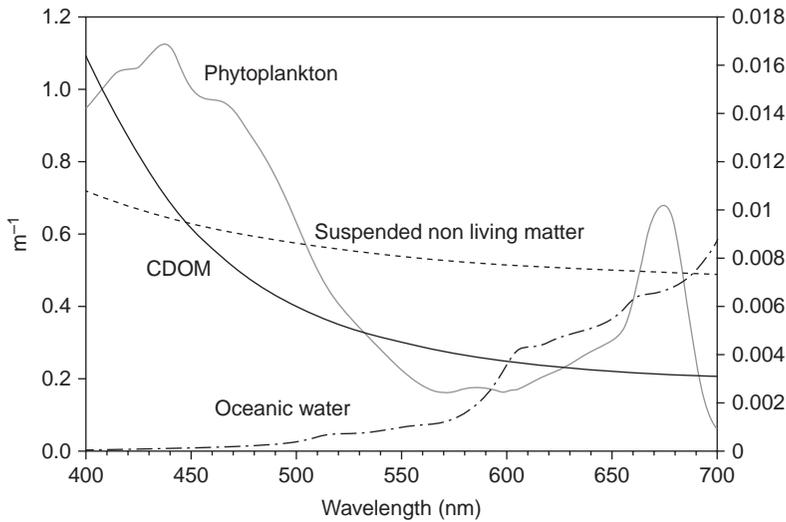
20.2 IOPs of clearest oceanic seawater (Pope and Fry, 1997), Chl *c* and Chl *b*-containing phytoplankton (Johnsen and Sakshaug, 2007, using Chl *a* concentration from experiment shown in Plate XXIII (see color section between pages 326 and 327) CDOM and suspended nonliving matter from Plate XXIII. Note that all spectra use the primary Y-axis (left), except phytoplankton that uses secondary Y-axis (right). Units: absorption, m^{-1}.

Hence, the spatial resolution capable from an underwater UHI is determined by both the intensity and spectral characteristics of the illumination source and the water clarity. For most applications, the distance between sensor and substrate must be measured with fairly high precision concomitantly with the imagery in order to account for light attenuation in the water column.

20.5.2. Optical correction of UHI

Two primary methods can be employed to correct for water column influences: (1) use of a reflectance plaque, or known reflectance target, that can be observed within the image itself; and (2) modeling of water column effects using knowledge of the inherent or AOPs of the water column. In the first approach, the ideal is to have a target with known reflectance properties situated at the same depth as the substrate within the sampled image. A target that reflects light equally at all wavelengths, such as spectralon, is considered optimal in order to make corrections across the entire visible spectrum, but is often too reflective for the radiometric response of the instrument and can saturate the detectors. A gray reference plaque is more appropriate for the low light conditions of the subsea. In theory, the sensed

radiance for each pixel can be normalized by the measured light scattered from a known target to account for the influence of the water column (e.g. Fig. 20.1a and 20.1b). In practice, situating a plaque at the same distance as the substrate is not practical from a moving ROV or AUV, and hence the plaque can be placed at a fixed distance from the sensor and the response numerically corrected assuming light attenuates exponentially (Equation [20.3]) and the water column is homogenous throughout the sampled layer. Challenges are inherent to having an external appendage with the plaque mounted on the vehicle, as well as keeping the plaque clean from debris (sediment deposition) and within the focal plane and the gain settings of the instrument (Fig. 20.3a and 20.3b).

In the second case, sensors can be deployed on the ROV or AUV to measure the optical properties of the water simultaneously with the image collection. Measured absorption and scattering properties can be input into radiative transfer equations to calculate the influence of the water column across each frame of the image. The advantage of this approach is that the full image swath can be reserved for subsea imaging of the OOI and not need to be obscured by a reference plaque. The disadvantage is that the instruments for estimating the full suite of IOPs are generally large in size and payload, requiring careful pre- and post-calibration (Twardowski *et al.*, 2005). Portable sensors that can be mounted on AUVs are available for measuring some of the required IOPs, more are in development, and proxy measurements (e.g. Chl *a* and CDOM fluorescence) can be coupled with bio-optical models to extend the required suite of instruments for the necessary corrections (Fig. 20.2).

The IOPs of the water column can be measured directly or the absorption and scattering properties can be inferred from measurements of the radiance field from depth, the AOPs. The rate of change of radiance and irradiance, known as the vertical diffuse attenuation coefficient (K, m^{-1}), is an AOP of the water column. Irradiance and radiance decrease approximately exponentially with depth, and can be related using Beer's Law. The downward diffuse attenuation coefficient, K_d, the rate of decrease in downwelling irradiance, $E_d(0)$, with depth (z):

$$E_d(z) = E_d(0)e^{-K_d z} \hspace{4cm} [20.3]$$

can be used to assess the influence of the water column on the imaged spectrum.

The orientation of the lamp with respect to the sensor, as well as the three-dimensional nature of the seabed or bidirectionality, will influence how much of the light hitting the seabed will scatter back in the direction of the sensor. Problems can also arise when using artificial lamps that may have variable illumination across the image swath. Cross-track illumination
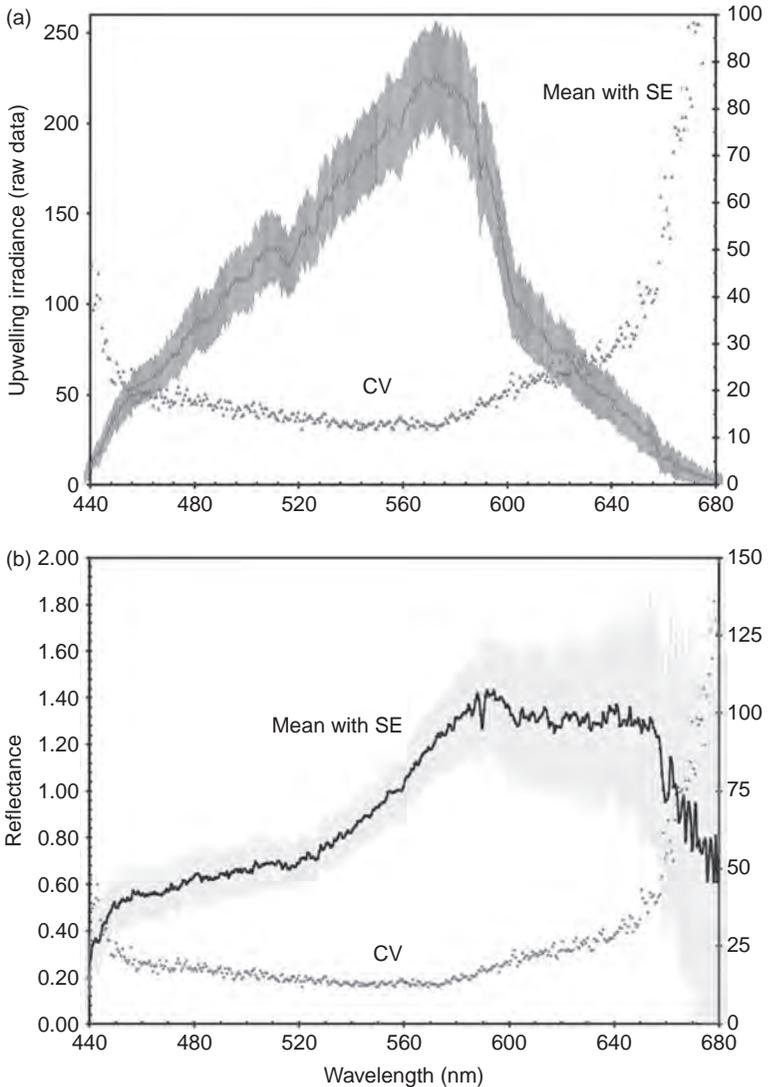
20.3 UHI data showing optical fingerprints from deep water corals from experiment illustrated in Plates XXIII–XXV and Fig. 20.4. (a) Raw data of upwelling irradiance, showing mean Eu(λ) to UHI detector (mean of 100 single point Eu(λ) spectra from 100 corresponding image pixels with standard error, SE, left Y-axis). CV denotes the coefficient of variation (CV) in % of mean Eu(λ), scale on right Y-axis. (b) The figure shows the corresponding reflectance, R(λ) corrected for IOP. Mean, SE and CV as in (a). The low values in the blue and red extremes is primarily due to low spectral sensitivity of the CCD from prototype UHI and high attenuation in the blue waveband (primarily due to CDOM) and in red (caused by high attenuation by water). For details, see Fig. 20.2 and Section 20.5.2.

effects and bidirectionality are both difficult to constrain, but do not generally alter the spectral distribution of light. Hence, imaging techniques outlined here may estimate the spectral shape of the bottom reflectance, but not the spectrum intensity (Gracias *et al.*, 2006, 2009).

Water column corrections are necessary when considering robust image processing approaches where little *in situ* knowledge is required and spectra can be compared to a predetermined library of optical fingerprints to characterize unknown features on the seafloor (Fig. 20.2). For regions known to have certain substrates a priori, spectral optimization approaches can be used to invert the measured radiance using a range of possible bottom types and IOPs and thereby produce accurate classifications of the imagery (Lee *et al.*, 1999, 2010).

If the aforementioned radiometric approaches are not possible, then potentially useful information can still be obtained from hyperspectral imagery with unsupervised techniques that result in maps of different 'types' of features. Such maps can be useful in marine reserves or other areas where the seabed features are already known and can be linked to the imagery by an informed decision maker. Routine monitoring at high spatial and spectral resolution afforded by subsea hyperspectral imagery, even with unsupervised techniques, can delineate temporal changes to habitats that are not easily detected with other methods (Plates XXIII–XXV (see in the color plate section between pages 326 and 327), Fig. 20.4).
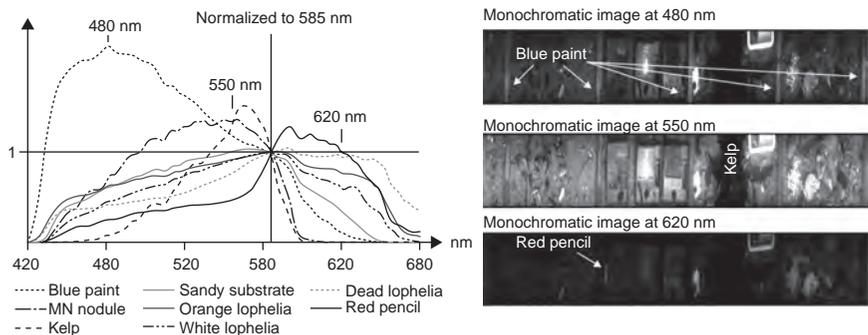
20.4 Optical fingerprints of OOI identified by UHI. The spectra is normalized at 585 nm, showing R(λ) for different OOI. Note blue paint with R(λ) maxima at 460–480 nm (blue by eye), kelp (*Laminaria digitata*) at 550–580 nm (green), and red pencil at 600–620 nm (bright red). Note that the deep water coral *Lophelia pertusa* obtains species-specific optical fingerprints and the UHI data could, in addition, discriminate between orange, white and dead corals. The Mn-nodules are characterized by optical fingerprints in blue-green, separating them from other OOI.

20.5.3   Optical classification algorithms

Once the water column influences have been quantified, the resulting bottom reflectance spectra can be matched to a spectral library of optical features using a variety of statistical approaches (Fig. 20.4 and Plate XXV in color section). Some methods are more sensitive to differences in spectral shape (i.e., dips and peaks in the spectra) and others to spectral magnitude (i.e., how light or dark the entire spectrum is). The derived bottom reflectance spectra may require normalization to render the spectra constant in magnitude and highlight only spectral shape differences. Hyperspectral datasets obtained under low signal conditions may also require filtering of spectral noise before processing (Fig. 20.4). Common classification approaches include parallelpiped, binary encoding algorithm, spectral angle mapper approaches, spectral information divergence, and minimum distance algorithm (Canty, 2007, Plate XXV). Compared to other methods, the spectral information divergence is better able to account for mixed pixels, made up of a combination of materials with different spectral signatures, and for variation in the signal due to atmospheric effects (Chang, 2003), and has been successfully applied to discriminate bottom types in a turbid estuary using hyperspectral imagery (Bostrom, 2011).

20.6   Applications of UHI-based biogeochemical seafloor mapping

20.6.1   Mapping of targeted biogeochemical objects of interest (OOI)

The optical fingerprints obtained from a hyperspectral imager serve as the basis for classification of OOI in a given digital seafloor map (Plates XXIII–XXV in color section, Fig. 20.4). The spectral fingerprints (Fig. 20.4) show examples of diverse constituents that may occur on a seabed, from natural to anthropogenic in origin. Blue paint with high reflectance maxima, R_{max}, at blue wavelengths (400–500 nm), can easily be separated from kelp with R_{max} in green and orange (550–600 nm). The cold-water coral *Lophelia pertusa* has an R_{max} at longer wavelengths into the red portion of the visible spectrum (Fig. 20.4). With the known optical fingerprints, automated approaches can then be applied to the imagery to conduct *de novo* OOI identification (Elde *et al.*, 2012). A monochromatic image can be produced at a given wavelength to highlight the color differences inherent to different OOIs (Fig. 20.4). Or, the entire image can be processed based on each OOI-specific optical fingerprint and used to produce coherent maps of objects on the seafloor in frame 1–4 (Plate XXIV). An example of detailed analysis of optical fingerprints from frame 2 is detailed in Plate XXV.

In this example, selected biological and anthropogenic OOI were imaged using an underwater cart and cart-track to simulate movements of ROV or AUV (Plate XXIIIa–XXIIIc in color section). The UHI survey site was Hopavågen (NTNU-field station Sletvik (63°35′32.94″N, 9°32′28.49″E) on a seafloor substrate characterized by fine sand and stones (1–10 cm). Scuba divers placed the custom-made UHI-carrying cart on the seafloor (Plate XXIIIa). The cart-track was divided in four sections (frames 1 to 4, each of 1×0.6 m), in a downhill slope at 4–5 m depth. Consistent movement of the trolley was achieved by using an electrical car winch powered with a 12 V car battery. The cart was connected to the winch with a 5 mm thick wire at a speed of 0.07 m s^{-1}. The UHI-cart was equipped with two halogen and two LED light sources (Green Force 35 W halogen lamp and Quadro LED lamp with depth rating of 500 m, Plexi IV battery with depth rating 200 m, 12 V, 13 Ah).

The UHI was used as a custom-made push-broom scanner (along track scanner) positioned with the image slit perpendicular to the moving direction according to Volent *et al.* (2007, 2009).

A custom-made underwater house holding 500 m of pressure and with glass (type BK7) for the optical window was used (Plate XXIII). The UHI was a small (25 cm long, 4 cm wide), light weight (620 g), solid state (no moving parts), low power requirement (12V, 0.16 Ah) push-broom sensor.

The UHI image frame rate was set to 25 images per second and was equipped with a 12 mm Schneider (f. 1.2) front lens with aperture set to 2.8 to enhance depth of field. The swath width (view-angle) at 1.35 m distance (optically 1.0 m in water) from the substrate was 40 cm and the spectral resolution was 1 nm spanning 420–680 nm. An underwater cable of 50 m was connected to the UHI for on-line monitoring, power (12 V battery), recording, exposure control, and data storage using a digital video recorder (Archos AV-400). The data from UHI were stored as video files (avi format) on a video recorder (13 Mb min^{-1}), comprising 25 images at 300 wavelengths giving an image cube of 7500 slit images s^{-1}.

Post-processing of UHI data and image analyses (Fig. 20.4, Plate XXIV in color section) were done with the custom-made yaPlaySpecX and Image calculator software described in Volent *et al.* (2007) and ENVI software (ITT Visual Systems Inc.). To exemplify image raw data analysis, 100 single point $E_u(\lambda)$ from a given OOI image pixel were used to calculate the mean $E_u(\lambda)$, its standard deviation (SD) and coefficient of variation (CV%), Fig. 20.3a. $E_u(\lambda)$, corrected for the spectral distribution of the ambient and underwater lamps by normalizing each pixel to the spectral distribution of the lamps, gives an OOI optical fingerprint corrected for ambient light, i.e. $R(\lambda)$ (Fig. 20.3b).

OOI in each frame represent different habitats, as follows (Fig 20.4, Plates XXIV and XXV in color section between pages 326 and 327):

Frame 1 represents natural seafloor habitat and fauna (Black Brittle stars, *Ophiocominanigra*), shell, sand, and stones. Frame 2: minerals (e.g. manganese nodules), metals, and bottom substrates with different elemental composition (see details in Plate XXV). Frame 3: The kelp species *Laminaria digitata* (from Trondheimsfjord), *L. solidungula* (from Svalbard) and reference plates (white). Frame 4: Orange and white living morphotypes and dead specimens of the reef building cold-water stony coral *Lophelia pertusa*, orange sponge (*Isodycthia palmata*), the giant file clam *Acesta excavata*, and the horny coral *Primnoa resedaeformis*.

Sampling of OOI found in frame 4 was carried out using ROV (100–4000 m depth) or by scuba diving (2–30 m depth). Biological OOI (cold-water corals, sponges, mussels) were sampled using a Sperre Subfighter 7500 ROV at 100–520 m depth at Stokkbergneset, Trondheimsfjord, Norway (63°28′N and 9°55′E). Mineral nodules were sampled from the eastern part of Clarion-Clipperton Zone in the Pacific (13°0′N and 127°0′W) at 4400 m depth in 2009 using a grab. Substrates with different loads of minerals and bacteria were made in the laboratory and later placed on the seafloor using SCUBA divers.

20.6.2   Mapping of seafloor substrates and chemical composition

Hyperspectral remote sensing has been used to identify and map specific chemical patterns on land and is useful for studying geology, soil chemistry, and mining (Hungate *et al.*, 2008). The composition in the structure of metallic oxides highly affects the visible and infrared reflectivity (Chasserio *et al.*, 2007; Hungate *et al.*, 2008). Hyperspectral information reflected from such targets may also allow for *in situ* detection of key minerals and their basic composition on the sediment surface of deep waters. However, determining the *in situ* spectral reflectance of the geochemical characteristics of different types of minerals and sediment surfaces under the impact of natural and human-made pressures is a challenging activity. As demonstrated above, progress has been made in determining the optical fingerprints of various sediments and substrates on the seafloor, and spectral libraries are being compiled for different sediment types. Such investigations, however, can be expanded from basic types of sediment (e.g. carbonate and mud) to elucidate the chemical compounds within the substrate.

Here we provide one example of how UHI may be used for monitoring chemical compounds near the seabed or along man-made pipelines. Carbon dioxide capture and storage in sub-seabed aquifers has been considered one of the most realistic CO_2 mitigation technologies (c.f. Mace *et al.*, 2007). In order to proceed with sub-seabed CO_2 storage technology, however, the 'London Protocol 2007' (see Mace *et al.*, 2007) includes a mandatory requirement for monitoring of such aquifers to detect both the possible

Table 20.1 Enrichment factors (in parenthesis) of some elements (ranking order) in nodules in Plate XXV (see color section between pages 326 and 327) compared to average elemental values of Crust

Samples	1	2	3	4
	Tl (271)	Tl (211)	Cu (160)	Cu (147)
	Cu (175)	Cu (175)	Cd (133)	Mn(143)
	Mn(148)	Cd (150)	Mn(106)	Tl (124)
	Cd (127)	Mn(101)	Ni (84)	Cd (109)
	Ni (96)	Ni (96)	Tl (77)	Mo (93)

Tl = thallium, Cu = copper, Mn = manganese, Cd = cadmium, Ni = nickel, and Mo = molybdenum.

CO_2 seepage and the potential impact on the sediment biogeochemistry. Monitoring low flux and episodic CO_2 seepage using traditional chemical methods is challenging given the subsea location and low concentrations. Changing geochemical characters of the sediment surface after long but low flux CO_2 seepage can be used as signatures of CO_2 seepage. The optical fingerprint from the sediment may change upon exposure to low amounts of CO_2. Hence, UHI could be a potential alternative for direct methods, which are incomplete for spatial coverage and extremely time consuming for monitoring low flux and episodic CO_2 seepage and its effects.

To investigate whether UHI could detect changes in geochemistry, we studied manganese nodules and different substrates with different minerals such as manganese oxide (MnO_2), manganese sulfate ($MnSO_4$), ferric oxide (Fe_2O_3), and ferric sulfate ($FeSO_4$). Ferric or iron compounds provide a reddish color to sediment, and the amount of iron can change the reflectance properties of the sediment (Dierssen *et al.*, 2006; Ardelan *et al.*, 2009; Ardelan and Steinnes, 2010, see details in Plate XXV).

Our preliminary results showed that there is distinct difference in optical fingerprints and elemental composition of Mn nodules relative to surrounding substrates (Table 20.1 and Plate XXV in color section). These elemental changes may be discriminated based on their spectral signature with UHI or other spectrophotometric techniques, leading toward automated seafloor identification and mapping of minerals of interest.

Sediment with various $CaCO_3$ content has also been analyzed to evaluate the impact of CO_2 seepage on sediment reflectance. Calcium carbonate minerals are highly reflective and cause enhanced reflectance across the visible spectrum (Dierssen *et al.*, 2009). Moreover, calcium carbonate is highly sensitive to the alkalinity of the water column (Feely *et al.*, 2009) and may undergo dissolution when exposed to CO_2. Seeps of CO_2 from beneath or near the seabed may lead to a decrease in carbonate content and subsequent decrease in reflectance within sediment that can be detected with UHI. Preliminary results indicate rapid reductions in the pH of surface sediment

after exposure to CO_2 seepage and could impact the reflectance properties of the sediment. However, since the reflectance spectra of carbonate is fairly 'white,' changes in carbonate content will have little impact on the spectral distribution of light emitted from the seafloor, but may change the amount of reflected light. For such applications, optical correction of the UHI is mandatory (see Section 20.5.2) in order to detect potential changes in the magnitude of the reflected signal. Routine surveys could be conducted to first determine a baseline seafloor reflectivity of a region in order to detect subtle changes in reflectivity that may be due to pH changes from CO_2 seeps.

20.6.3   UHI for marine mining applications

Airborne hyperspectral surveying is now a standard tool for the mining industries on land. Minerals can be identified based on their visible and infrared spectral reflectances (Jefferson Lab, 2007). However, the greatest unexploited mineral resources on earth are on the deep-sea floor, including hydrothermal deposits, manganese nodules, and cobalt-rich manganese crusts (Glasby, 2000). Hydrothermal deposits or seafloor massive sulfide (SMS) deposits, are forming in the deep ocean around submarine volcanic arcs, where hydrothermal vents exhale sulfide-rich mineralizing fluids into the ocean. SMS deposits contain appreciable grades of Cu, Pb, Zn, Ag, Au, and other trace metals (Hein, 2000). Hydrothermal deposits are typically found at a depth of 1500–3000 m (Cronan, 2000).

Polymetallic nodules, also called manganese nodules, are rock concretions on the sea bottom formed of concentric layers of iron and manganese hydroxides around a core (Cronan, 2000; Tan *et al.*, 2006). These typically contain manganese, nickel, copper, cobalt, iron, silicon and aluminum, with lesser amounts of calcium, sodium, magnesium, potassium, titanium, and barium (Achurra *et al.*, 2009). Manganese nodules are typically half-buried in comparatively flat deep-sea sediment at a depth of 4000–6000 m (see details Plate XXV).

Cobalt-rich manganese crusts are found throughout the global oceans at depths of 800–2400 m on the flanks and summits of seamounts, ridges, and plateaus, where seafloor currents have swept the ocean floor clear of sediment for millions of years. The minerals in crusts have precipitated out of the cold ambient seawater onto the rock surface and form pavements up to 25 cm thick and cover an area of many square kilometers. In addition to manganese and cobalt, crusts are an important potential source for many other metallic and rare earth elements, such as titanium, cerium, nickel, platinum, manganese, phosphorus, thallium, tellurium, zirconium, tungsten, bismuth, and molybdenum (Glasby, 2000, 2006).

UHI has potential for identifying and characterizing different deposits for underwater mining applications (Plate XXV). Often minerals are remotely sensed using absorption features in the infrared portion of the

spectrum (2–2.5 μm, Kruse, *et al.*, 2003). The infrared portion of the spectrum, however, is highly absorbed by water (Fig. 20.2) and such features are not generally observable with passive airborne remote sensing of the seafloor. Near-infrared photons measured by a satellite sensor, for example, are commonly attributed to atmospheric scattering from aerosols and not usable for water applications (Dierssen and Randolph, 2013). However, with lamps enriched in red photons, UHI techniques may be able to exploit some of these spectral features in longer wavelengths and have additional applications for mineral mapping of the seabed. This would be useful both during prospecting for minerals and during mining itself, as an underwater hyperspectral imager should be capable of both identifying deposits, quantifying and classifying ore content.

20.7   Acknowledgements

20.8   References

Achurra L E, Lacassie J P, Le Roux J P, Marquardt C, Belmar M, Ruiz-del-Solar J and Ishman S E (2009), ' Manganese nodules in the Miocene BahaInglesa Formation, north-central Chile: petrography, geochemistry, genesis and palaeoceanographic significance', *Sedimentary Geology*, **217**, 128–139.

Ardelan M V, Steinnes E, Lierhagen, S and Linde, S O (2009), 'Effects of experimental CO_2 leakage on solubility and transport of seven trace metals in seawater and sediment', *Science of the Total Environment*, **407**, 6255–6266.

Ardelan M V and Steinnes E (2010), 'Changes in mobility and solubility of the redox sensitive metals Fe, Mn and Co at the seawater-sediment interface following CO_2 seepage', *Biogeosciences*, **7**, 569–583.

Barker B A J, Helmond I, Bax N J, Williams A, Davenport S and Wadley V A (1999), 'A vessel-towed camera platform for surveying seafloor habitats of the continental shelf', *Continental Shelf Research*, **19**, 1161–1170.

Bierwirth P N, Lee T J and Burne R V (1993), 'Shallow sea floor reflectance and water depth derived by unmixing multispectral imagery', *Photogrammetric Engineering and Remote Sensing*, **59**(3), 331–338.

Blackwell S M, Moline M A, Schaffner A, Garrison T and Chang G (2007), 'Subkilometer length scales in coastal waters', *Continental Shelf Research*, **28**, 215–226, doi:10.1016/j.csr.2007.07.009.

Blough N V and Del Vecchio R (2002), Chromophoric DOM in the coastal envi-
ronment, In: *Biogeochemistry of Marine Dissolved Organic Matter*, San Diego,
Academic Press, XXII, 509–546.

Bostrom K (2011), 'Testing the limits of hyperspectral airborne remote sensing by
mapping eelgrass in Elkhorn Slough', M.S. Thesis, University of Connecticut.

Bricaud A, Claustre H, Ras J and Oubelkheir K (2004), 'Naural variablility of
phytoplanktonic absorption in oceanic waters: Influence of the size struc-
ture of algal populations', *Journal of Geophysical Research*, **106**, C11010,
doi:10.1029/2004JC002419.

Boyd S E, Coggan R A, Birchenough S N R, Limpenny D S, Eastwood PE, Foster-
Smith R L, Philpott S, Meadows, James J W C, Vanstaen K, Soussi S and Rogers
S (2006), 'The role of seabed mapping techniques in environmental monitoring
and management', *Science Series Technical Report*, Cefas, Lowestof, **127**, 170.

Buhl-Mortensen L, Hodnesdal H and Thorsnes T (2010), *Til bunns i Barentshavet
og havområdene utenfor Lofoten (In Norwegian with english summary)*,
Trondheim, Norway, Norges Geologiske Undersøkelse,128.

Buonassissi C and Dierssen H M (2010), 'A regional comparison of particle size distribu-
tions and the power-law approximation in oceanic and estuarine surface waters',
Journal of Geophysical Research, **115**, C10028. doi:10.1029/2010JC006256.

Canty M J (2007), *Image Analysis, Classification, and Change Detection in Remote
Sensing: with Algorithms for ENVI/IDL*, CRC/Taylor and Francis, Boca Raton,
London, New York, 348 pp.

Chang C I (2003), *HyperspectralImaging: Techniques for SpectralDetection and
Classification*, NewYork, Kluwer Academic/PlenumPublishers.

Chasserio N, Durand B, Guillemet S and Rousset A (2007), 'Mixed manganese spi-
nel oxides: optical properties in the infrared range', *Journal of Materials Science,*
42, 794–800.

Cronan D S (ed.) (2000), *Handbook of Marine Mineral Deposit's*, CRC Press, London.

Davis C. O, Carder K L, Gao B C, Lee Z-P and Bissett W P (2006),'The develop-
ment of imaging spectrometry of the coastal ocean', In: *IEEE International
Conference on Geoscience and Remote Sensing Symposium, IGARSS 2006*,
Denver, Colorado, USA, 1982–1985.

Dierssen H M (2010), 'Benthic ecology from space: optics and net primary produc-
tion in seagrass and benthic algae across the Great Bahama Bank', *Marine
Ecology Progress Series*, **411**, 1–15. doi:10.3354/meps08665.

Dierssen H M and Randolph K (2013), Remote sensing of ocean color, In:
Encyclopedia of Sustainability Science and Technology, Springer, In press.

Dierssen H M, Kudela R M, Ryan J P and Zimmerman R C (2006), 'Red and black
tides: Quantitative analysis of water-leaving radiance and perceived color for
phytoplankton, colored dissolved organic matter, and suspended sediments',
Limnology and Oceanography, **51**(6), 2646–2659.

Dierssen H M, Zimmerman R C and Burdige D J (2009), 'Optics and remote sensing
of Bahamian carbonate sediment whitings and potential relationship to wind-
driven Langmuir circulation', *Biogeosciences*, **6**(3), 487–500.

Dierssen H M, Zimmerman R C, Leathers R A, Downes T V and Davis C O (2003),
'Ocean color remote sensing of seagrass and bathymetry in the Bahamas Banks by
high resolution airborne imagery', *Limnology and Oceanography*, **48**, 456–463.

Elde A, Pettersen R, Bruheim P, Järnegren J and Johnsen G (2012), 'Pigmentation and
spectral absorbance signatures in deep-water corals from the Trondheimsfjord,
Norway', *Marine Drugs*, **10**, 1400–1411.

Fearns P R C, Klonowski W, Babcock R C, England P, and Phillips J (2011), 'Shallow water substratemapping using hyperspectral remote sensing', *Continental Shelf Research*, **31**(12), 1249–1259.

Feely R A, Doney S C and Cooley S R (2009), 'Ocean acidification: Presentconditions and future changes in a high-CO_2 world', *Oceanography*, **22**(4), 36–47.

Gintert B, Gracias N, Gleason ACR, Lirman D, Dick M, Kramer P and Reid R P (2009), Second-Generation Landscape Mosaics of Coral Reefs, *Proceedings of the 11th International Coral Reef Symposium*, Ft. Lauderdale, Florida, 577–581 (Conference 7–11 July 2008).

Glasby GP (2000), Manganese: predominant role of nodules and crusts, In: Schulz H D and Zabe M (eds.), *Marine Geochemistry*, Springer, Berlin, 335–372.

Glasby G P (2006), Manganese: predominant role of nodules and crusts, In: Schulz H D and Zabe M (eds.), *Marine Geochemistry*, Springer, Berlin, 335–372.

Gleason A C R, Gracias N, Lirman D, Gintert B E, Smith T B, Dick M C and Reid R P (2010), 'Landscape video mosaic from a mesophotic coral reef', *Coral Reefs*, **29**(2), 253. doi: 10.1007/s00338–009–0544–2.

Gleason A C R, Lirman D, Williams D, Gracias N R, Gintert B E, Madjidi H, Reid R P, Boynton G C, Negahdaripour S, Miller M and Kramer P (2007), 'Documenting hurricane impacts on coral reefs using two-dimensional video-mosaic technology', *Marine Ecology*, **28**, 254–258.

Gleason A C R, Reid R P and Voss K J (2007), Automated classification of underwater multispectral imagery for coral reef monitoring, *Proceed MTS/IEEE Oceans* (Conference 1–4 October 2007), Vancouver, Canada.

Gracias N R, Gleason A, Negahdaripour S and Mahoor M (2006), Fast Image Blending using Watersheds and Graph Cuts, *Proceedings of the British Machine Vision Conference*, Edinburgh, paper #259, UK (Conference 4–7 September 2006).

Gracias N R, Mahoor M, Negahdaripour S and Gleason A (2009), 'Fast image blending using watersheds and graph cuts', *Image and Vision Computing*, **27**(5), 597–607. doi: 10.1016/j.imavis.2008.04.014

Grahn H F and Geladi P (2007), *Techniques and Applications of Hyperspectral Image Analysis*, New York, Wiley & sons. DOI: 10.1002/9780470010884.

Hein J (2000), Cobalt-rich ferromanganese crusts: global distribution, composition, origin and research activities, in workshop on mineral resources of the International Seabed Area, Kingston, Jamaica, 26–30 June 2000.

Hochberg E and Atkinson M J (2003), 'Capabilities of remote sensors to classify coral, algae, and sand as pure and mixed spectra', *Remote Sensing of Environment*, **85**, 174–189.

Hungate W S, Watkins R and Borengasser M (2008), *Hyperspectral Remote Sensing; Principles and Applications*, CRC Press, 101–112.2008 DOI: 10.1201/9781420012606.ch10.

IOCCG (2008), Why ocean colour? The societal benefits of ocean-colour technology. In Platt T, Hoepffner N, Stuart V and Brown C. (eds.), *Reports of the International Ocean-Colour Coordinating Group*, No. 7, IOCCG, Dartmouth, Canada.

Jefferson Lab (2007), It's Elemental – The Periodic Table of Elements. Available from: http://education.jlab.org/itselemental.htm (Accessed 14 August 2007).

Johnsen G and Sakshaug E (2007), 'Bio-optical characteristics of PSII and PSI in 33 species (13 pigment groups) of marine phytoplankton, and the relevance for PAM and FRR fluorometry', *Journal of Phycology*, **43**, 1236–1251.

Johnsen G, Volent Z, Sakshaug E, Sigernes F, Pettersson L H (2009), Remote sensing in the Barents Sea, In: Sakshaug E, Johnsen G and Kovacs K (eds.), *Ecosystem Barents Sea*, Trondheim, Norway, Tapir Academic Press, 139–166.

Johnsen G, Moline M, Pettersson L H, Pinckney J, Pozdnyakov D V, Egeland E and Schofield O M (2011), Optical monitoring of phytoplankton bloom pigment signatures, In: Roy S, Llewellyn C, Egeland E and Johnsen G (eds.), *Phytoplankton pigments: Updates on Characterization, Chemotaxonomy and Applications in Oceanography*, Cambridge University Press, Chapter 14, 538–581.

Kirk J T O (1994), *Light and Photosynthesis in Aquatic Ecosystems*, Cambridge University Press, Cambridge.

Klonowski W M, Fearns P R C S and Lynch M R (2007), 'Retrieving key benthic cover types and bathymetry from hyperspectral imagery', *Journal of Applied Remote Sensing*, **1**, 011505.

Kongsberg Maritime (2004), APOS Basic Operator Course, in Horten, Kongsberg Maritime: 210. Available from: http://www.km.kongsberg.com

Kruse F A, Boardman J W and Huntington J F (2003), 'Comparison of airborne hyperspectral data and EO-1 Hyperion for mineral mapping', *Geoscience and Remote Sensing, IEEE Transactions on*, **41**(6), 1388–1400.

Lee Z P, Hu C, Casey B, Shang S, Dierssen H and Arnone R (2010), 'Global shallow-water high resolution bathymetry from ocean color satellites', *EOS Trans. Amer. Geophy. Union*, **91**(46), 429–430.

Lee Z, Carder K L, Mobley C D, Steward R G and Patch J S (1999), 'Hyperspectral remote sensing for shallow waters. 2. deriving bottom depths and water properties by optimization', *Applied Optics*, **38**(18), 3831–3843.

Lucke R L, Corson M, McGlothlin N R, Butcher S D, Wood D L, Korwan D R, Li R R, Snyder W A, Davis C O and Chen D T (2011), 'Hyperspectral Imager for the Coastal Ocean: instrument description and first images', *Applied Optics*, **50**(11), 1501–1516.

Ludvigsen M, Sortland B, Johnsen G and Singh H (2007), 'The use of geo-referenced underwater photo-mosaics from ROV in marine biology and archaeology', *Oceanography*, **20**, 74–83.

Mace M J, Hendriks C and Coenraads R (2007), 'Regulatory challenges to the implementation of carbon capture and geological storage within the European Union and international law', *International Journal of Greenhouse Gas Control*, **1**, 253–260.

Marshall N J and Oberwinkler J (1999), 'The colourful world of the mantis shrimp', *Nature*, **401**, 873–874.

Marshall J, Cronin T W and Kleinlogel S (2007), 'Stomatopod eye structure and function: A review', *Arthropod Structure and Development*, **36**, 420–448.

Milne P H (1983), *Underwater Acoustic Positioning Systems*. Cambridge, Great Britain University Press.

Mobley C D, Sundman L K, Davis C O, Bowles J H, Downes T V, Leathers R A, Montes M J, Bissett W P, Kohler D D R, Reid R P, Louchard E M and Gleason A (2005), 'Interpretation of hyperspectral remote-sensing imagery by spectrum matching and look-up-tables', *Applied Optics*, **44**(17), 3576–3592.

Moline M A, Blackwell S M, Allen B, Austin T, Forrester N, Goldsborogh R, Purcell M, Stokey R and von Alt C (2005), 'Remote environmental monitoring units: an autonomous vehicle for characterizing coastal environments', *Journal of Atmospheric and Oceanic Technology*, **22** (11), 1798–1809.

Moline M A, Woodruff D L and Evans N R (2007), 'Optical delineation of benthic habitat using an autonomous underwater vehicle', *Journal of Field Robotics*, **24** (6), 461–471.doi: 10.1002/rob.20176.

Mouroulis P, Van Gorp B E, Green R O, Eastwood M, Wilson D W, Richardson B and Dierssen H (2012), 'The Portable Remote Imaging Spectrometer (PRISM) coastal ocean sensor', Optical Remote Sensing of the Environment Conference paper, Monterey, California United States, 24–28 June 2012, New Uses of Optical Remote Sensing.

Phinn S R, Dekker A G, Brando V E and Roelfsema C M (2005), 'Mapping water quality and substrate cover in optically complex coastal and reef waters: an integrated approach', *Marine Pollution Bulletin*, **51**(1–4), 459–469.

Pope R and Fry E (1997), 'Absorption spectrum of pure water: 2. Integrating cavity measurements', *Applied Optics*, **36**(33), 8710–8723.

Ryan J, Dierssen H M, Kudela R M, Scholin C A, Johnson K S, Sullivan J M, Fischer A M, Rienecker E V, McEnaney P R and Chavez F P (2005), 'Coastal ocean physics and red tides', *Oceanography*, **18**, 246–255.

Singh H, Howland J and Pizzaro O (2004a),'Advances in large-area photomosaicking underwater', *IEEE Journal of Oceanic Engineering*, **29**, 872–886.

Singh H, Can A, Eustice R, Lerner, S, McPhee N, Pizarro O and Roman C (2004b), 'Sea BEDAUV offers new platform for high-resolution imaging', *EOS, Transactions of the AGU*, 85(31), 289, 294–295.

Sosik H M, Olson R J, Neubert M G, Shalapyonok A and Solow A R (2003), 'Growth rates of coastal phytoplankton from time-series measurements with a submersible flow cytometer', *Limnology and Oceanography*, **48**, 1756–1765.

Tan W F, Liu F, Li Y H, Hu H Q and Huang Q Y (2006), 'Elemental composition and geochemical characteristics of iron-manganese nodules in main soils of China', *Soil Science Society of China*. doi:10.1016/S1002–0160(06)60028–3.

Twardowski M S, Lewis M, Barnard A and Zaneveld J R V (2005), In-water instrumentation and platforms for ocean color remote sensing applications, In *Remote Sensing of Coastal Aquatic Waters*, Springer, Dordrecht, Netherlands.

Volent Z, Johnsen G and Sigernes F (2007), 'Kelp forest mapping by use of airborne hyperspectral imager', *Journal of Applied Remote Sensing*, **1**, 011503.

Volent Z, Johnsen G and Sigernes F (2009), 'Microscopic hyperspectral imaging used as bio-optical taxonomic tool for micro- and macroalgae', *Applied Optics*, **48**, 4170–4176.

Volent Z, Johnsen G, Hovland E K, Folkestad A, Olsen L M and Tangen K (2011), 'Improved monitoring of phytoplankton bloom dynamics in a Norwegian fjord by integrating satellite data, pigment analysis and Ferrybox data with a coastal observation network', *Journal of Applied Remote Sensing*, **5**, 053561, doi:10.1117/1.3658032.

Williams S B, Pizarro O, Webster J M, Beaman R J, Mahon I, Johnson-Roberson M and Bridge T (2010), 'Autonomous underwater vehicle-assisted surveying of drowned reefs on the shelf edge of the Great Barrier Reef, Australia', *Journal of Field Robotics*, **27**, 675–697.

Williams S B, Pizarro O, Mahon I and Johnson-Roberson M (2008), 'Simultaneouslocalisation and mapping and dense stereoscopic seafloor reconstruction using an AUV', In: *Proc. of the Int'l Symposium on Experimental Robotics*, 13–16 July, Athens, Greece.
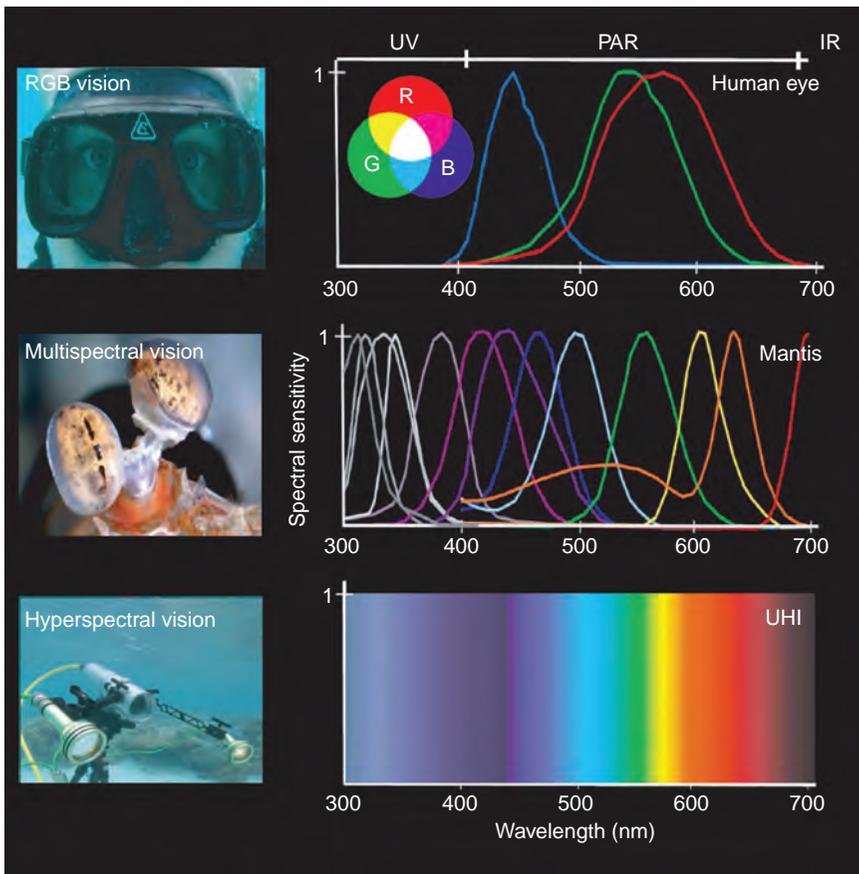
Plate XIX (Chapter 20) Principles of trichromatic (RGB) human eye vs multispectral (mantis shrimp) and hyperspectral vision. (Source: Upper and mid images and graphics are modified from Marshall and Oberwinkler, 1999; Marshall, *et al.* 2007. Photos: Upper and lower picture by Geir Johnsen. Middle image of mantis shrimp by Roy Caldwell, University of California, Berkeley, with permission.)
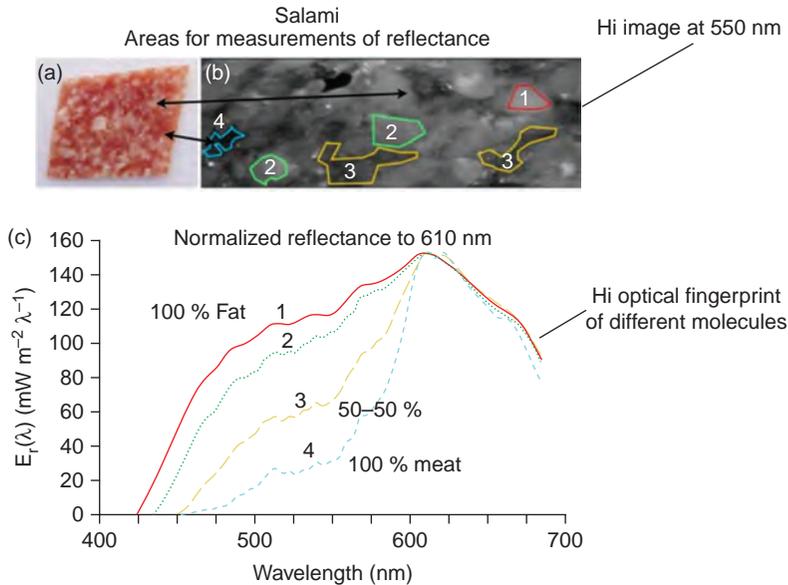
Plate XX (Chapter 20) Principles of hyperspectral imaging (HI) discriminating between chemical composition (fat vs meat) in a salami sausage. (a) Ordinary photo (RGB). (b) HI image from microscope (4 × magnification) at reflectance of 550 nm, and (c) hyperspectral optical fingerprints (R(λ)) of fat, meat and blend of fat and meat illustrating 'chemical imaging'. Er (λ) denotes upwelling irradiance. Area 1–4 indicates different percentage of fat vs meat.
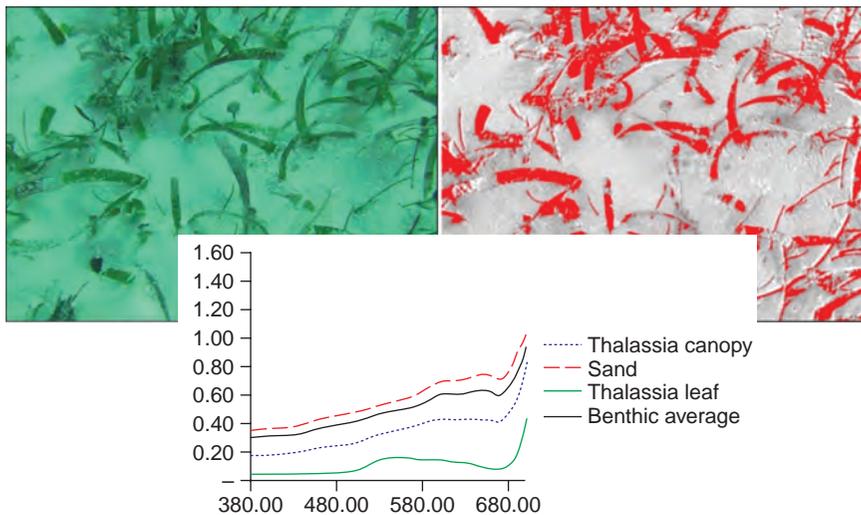

Plate XXI (Chapter 20) Leaves of the seagrass *Thalassia testudinum* growing in the bright carbonate sand in Greater Florida Bay. Images of the benthos can be classified in order to determine the average reflectance of the seafloor over large spatial scales for productivity and biogeochemistry of seagrass meadows (e.g. Dierssen *et al.*, 2010).

© Woodhead Publishing Limited, 2013

(a)

(b)
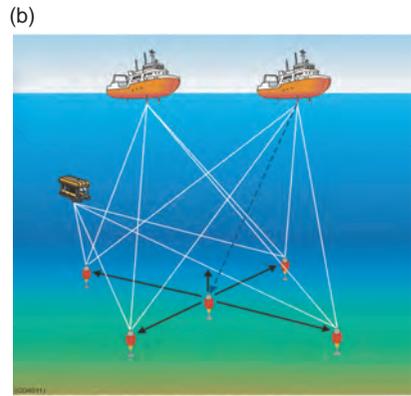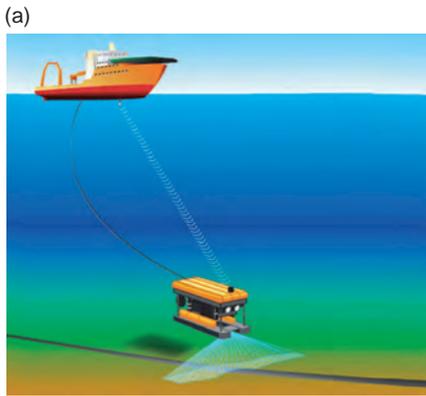
Plate XXII (Chapter 20) Acoustic underwater navigation of underwater robots with UHI mounted for geo-referencing. (a) Ultra Short BaseLine (USBL) and (b) Long BaseLine (LBL). To achieve a global position using a USBL system a ship mounted transceiver, a ship mounted orientation sensor, a GPS a transponder mounted on the ROV is required. (Source: By permission, Kongsberg Maritime, 2004.)


(a)

(b)

R 581 nm

Scale 4m
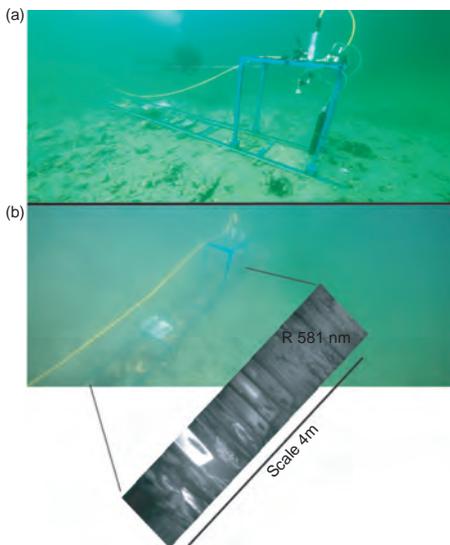
UHI image reflectance at 581 nm of objects of interest (OOI)

Plate XXIII (Chapter 20) Set up of an UHI prototype seafloor mapping of biogeochemical OOI in April 2010 in Hopavågen, Norway. (a) The UHI was mounted on an underwater cart with artificial light sources and the scene being observed. The light signal detected at the UHI is a combination of light reflected from the OOI and light scattered in the intervening light path. The light from the light source is reflected by the OOI and then transmitted directly to the sensor that represents the spectral signature of the OOI. (b) Shows 4 frames with different substrates, minerals, manganese nodules, animals (e.g. frame 4 with corals, sponges, brittle stars, sea stars, kelp, mussels). For details, see Section 20.6 and Fig. 20.4 and Plates XXIV XXV.

(a) UHI rawdata:

Raw UHI data at R of 560 nm. scale bar = 4 m
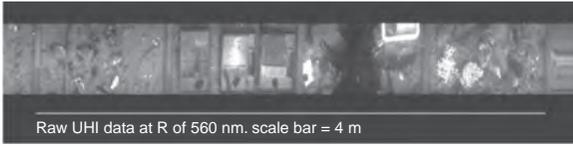
UHI based RGB image:
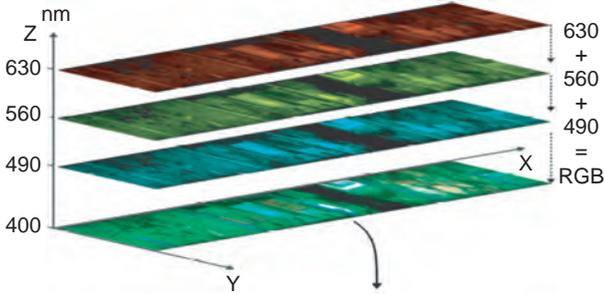
(b) Frame 1   Frame 2   Frame 3   Frame 4

UHI RGB
UHI 560 nm
Classification of OOI
Classification on RGB
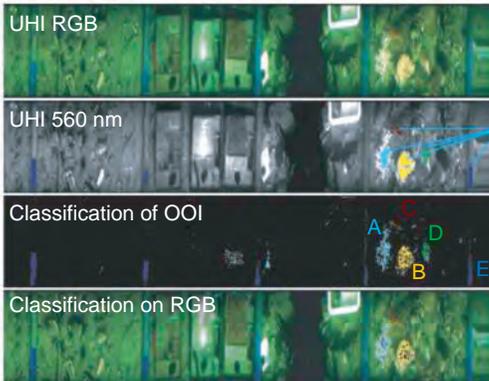
UHI RGB image (490,560 & 630 nm):
To generate a "colour image".

UHI image at 560 nm:
specifying OOI to be classified.
Based on optical fingerprints of white & orange
Lophelia pertusa, orange sponge
(*Isodycthia palmata*), clam (*Acesta excavata*)
and blue paint.

Classification of OOI
White *Lophelia* (A)
Orange *Lophelia* (B)
Isodycthia (sponge, C)
Acesta (clam, D)
Blue paint (E)

Plate XXIV (Chapter 20) (a) Shows R at 560 nm, with corresponding
RGB images (at 490, 560 and 630 nm). When the RGB layers are put
together we obtain a full colour picture for the human eye (cf. Plate
XIX). (b) Indicates identification and area coverage of different OOI
based on specific optical fingerprints (R(λ)). For details, see Section
20.6.

Spectral angle mapper

Binary encoding
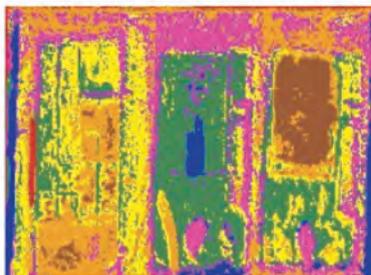
Spectral information divergence
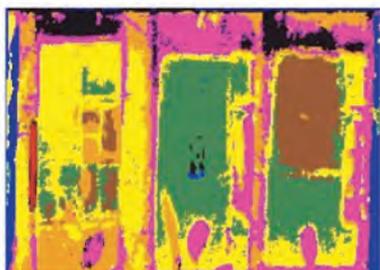
Minimum distance
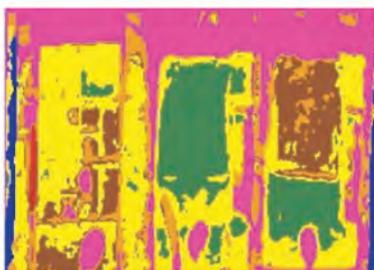
Plate XXV (Chapter 20) Detail of frame 2 shown in Plate XXIV, showing blue metal frame on seafloor (blue), rusted piece of iron (orange), Mn nodules (magenta), substrate 1 dominated by ferric sulfate, Fe(III) SO$_4$ (yellow, 10 in picture), substrate 2 is dominated by oxidized iron in sediment (brown, 18 in picture), substrate 3 consisting on ferric sulfate (upper part of frame, and below a substrate dominated by reduced manganese sulfate under Mn nodule (green, 19 in picture above Mn nodule), and red pencil (red). The substrates have different content of biofilm (benthic microalgae and bacteria), different element content (e.g. With oxidized Fe and Cu). Different algorithms have been deployed to identify OOI: Upper left (spectral angle mapper algorithm), upper right (binary encoding), lower left (spectral information divergence) and lower right (minimum distance).